AD A108808

DTIC FILE COPY

FTD-ID(RS)T-0927-81

2

FOREIGN TECHNOLOGY DIVISION

DTIC
ELECTE
DEC 23 1981
E

CALCULATION OF SUPERSONIC THREE-DIMENSIONAL FLOW ABOUT BLUNT-NOSED BODIES

by

Zhu Youlan, Wang Ruquan, and Zhong Xichang

Approved for public release;
distribution unlimited.

81 12 23 049

EDITED TRANSLATION

FTD-ID(RS)T-0927-81 19 November 1981

MICROFICHE NR: FTD-81-C-001049

CALCULATION OF SUPERSONIC THREE-DIMENSIONAL FLOW ABOUT BLUNT-NOSED BODIES

By: Zhu Youlan, Wang Ruquan, and Zhong Xichang

English pages: 24

Source: Peking Li-hsueh (Mechanics), Nr 4, 1977, pp. 270-282

Country of origin: China
Translated by: Randy Dorsey
Requester: FTD/TQTA
Approved for public release; distribution unlimited.

THIS TRANSLATION IS A RENDITION OF THE ORIGINAL FOREIGN TEXT WITHOUT ANY ANALYTICAL OR EDITORIAL COMMENT. STATEMENTS OR THEORIES ADVOCATED OR IMPLIED ARE THOSE OF THE SOURCE AND DO NOT NECESSARILY REFLECT THE POSITION OR OPINION OF THE FOREIGN TECHNOLOGY DIVISION.

PREPARED BY:

TRANSLATION DIVISION
FOREIGN TECHNOLOGY DIVISION
WP-AFB, OHIO.

Accession For
NTIS GRA&I
DTIC TAB
Unannounced
Justification
By
Distribution/
Availability Codes
Dist | Avail and/or Special
A

CALCULATION OF SUPERSONIC THREE-DIMENSIONAL FLOW ABOUT BLUNT-NOSED BODIES

by Zhu Youlan, Wang Ruquan, and Zhong Xichang
Chinese Academy of Sciences, Institute of Computer Technology

1. INTRODUCTION

From the latter part of the 50's to the present, many methods have appeared for finding a numerical solution to the problem of supersonic inviscid flow about blunt-nosed bodies. Of these, one type is classified as the non-stationary methods and the other type as the steady-state methods. Among the steady-state methods there is also the finite difference method, the integral relationship method, the straight-line method, etc. All of these methods relate to smooth objects and all can obtain satisfactory results. But, since the non-stationary method must undergo a process of stabilization with respect to time, the machine time expended is very great. In regard to the finite difference method, in order to obtain sufficiently accurate results, it is required that grid points cannot be too few, and thus machine storage capacity must be rather great. Also a large amount of computer time is expended. In comparison, the straight-line method has many advantages. For example, its algorithms are simple and the required storage capacity is small, and using very few rays makes it possible to obtain satisfactory results. This paper mainly describes our work in the field of supersonic flow about blunt-nosed bodies using the straight-line method of calculation.

We used the straight-line method to conduct extensive calculations of supersonic flow about blunt-nosed bodies. The calculated objects' shapes were ellipsoids with various axial ratios as well as objects which were nearly disc-shaped. The Mach numbers of the oncoming flow ranged from 1.5 to ∞. Under conditions of axial symmetry, calculations were carried out on not only frozen gas with $\gamma = 1.4$ but also on flow in equilibrium air and non-equilibrium air.

Furthermore, we also used the straight-line method to calculate flow in the supersonic region and flow with a sharp angle of attack.

We conducted many checks along the way on the calculated results. All of the checks indicated that the results obtained using the straight-line method were quite satisfactory.

2. FORMULATION OF THE PROBLEM

2.1 The basic equation

Inviscid and non-heat-conducting steady-state gaseous flows were taken into consideration. The aerodynamic equation in the spherical coordinate system (r, θ, φ) is

$$\left.\begin{aligned}
&\frac{1}{r^2\sin\theta}\left\{\frac{\partial}{\partial r}(\rho u r^2\sin\theta)+\frac{\partial}{\partial\theta}(\rho v r\sin\theta)+\frac{\partial}{\partial\varphi}(\rho w r)\right\}=0\\
&\frac{du}{dt}-\frac{v^2+w^2}{r}+\frac{1}{\rho}\frac{\partial p}{\partial r}=0\\
&\frac{dv}{dt}+\frac{uv}{r}-\frac{\operatorname{ctg}\theta}{r}w^2+\frac{1}{r\rho}\frac{\partial p}{\partial\theta}=0\\
&\frac{dw}{dt}+\frac{uw}{r}+\frac{\operatorname{ctg}\theta}{r}vw+\frac{1}{\rho r\sin\theta}\frac{\partial p}{\partial\varphi}=0\\
&\frac{dp}{dt}-c^2\frac{d\rho}{dt}=0
\end{aligned}\right\}\qquad(2.1)$$

where $\frac{d}{dt}=u\frac{\partial}{\partial r}+v\frac{1}{r}\frac{\partial}{\partial\theta}+w\frac{1}{r\sin\theta}\frac{\partial}{\partial\varphi}$, u, v, w, respectively, are the velocity components in the directions of r, θ, φ, p is pressure, ρ is density, and c is sonic velocity. All the quantities in the equation are dimensionless quantities and their dimensional factors are, respectively,

$$p\sim\rho_\infty V_\infty^2,\quad \rho\sim\rho_\infty,\quad u, v, w\sim V_\infty,\quad r\sim R_0$$

Here, subscript ∞ represents the quantity of oncoming flow and R_0 is the radius of curvature of the apex of the object's nose. In order to simplify calculation, we introduce the following coordination conversions:

$$\xi = \frac{r - G(\theta, \varphi)}{F(\theta, \varphi) - G(\theta, \varphi)}, \quad \theta = \theta, \quad \varphi = \varphi$$

where $r = G(\theta, \varphi)$ and $r = F(\theta, \varphi)$ are the equations for the object surface and shock wave, respectively. It is evident that in the (ξ, θ, φ) coordinate system the shock wave lies within the $\xi = 1$ plane and the object surface lies within the $\xi = 0$ plane. Let

$$\alpha = -(G_\theta + \xi\varepsilon_\theta), \quad \beta = -\frac{1}{\sin\theta}(G_\varphi + \xi\varepsilon_\varphi), \quad \varepsilon = F - G$$

and since

$$\frac{\partial}{\partial r} = \frac{1}{\varepsilon}\frac{\partial}{\partial \xi}, \quad \frac{\partial}{\partial \theta} = \frac{\alpha}{\varepsilon}\frac{\partial}{\partial \xi} + \frac{\partial}{\partial \theta}$$

$$\frac{1}{\sin\theta}\frac{\partial}{\partial \varphi} = \frac{\beta}{\varepsilon}\frac{\partial}{\partial \xi} + \frac{1}{\sin\theta}\frac{\partial}{\partial \varphi}$$

consequently, equation (2.1) can be written as

$$\left.\begin{aligned} &a\frac{\partial \rho}{\partial \xi} + \rho\left(r\frac{\partial u}{\partial \xi} + \alpha\frac{\partial v}{\partial \xi} + \beta\frac{\partial w}{\partial \xi}\right) = F_1, \quad a\frac{\partial u}{\partial \xi} + \frac{r}{\rho}\frac{\partial p}{\partial \xi} = F_2 \\ &a\frac{\partial v}{\partial \xi} + \frac{\alpha}{\rho}\frac{\partial p}{\partial \xi} = F_3, \quad a\frac{\partial w}{\partial \xi} + \frac{\beta}{\rho}\frac{\partial p}{\partial \xi} = F_4, \quad a\left(\frac{\partial p}{\partial \xi} - c^2\frac{\partial \rho}{\partial \xi}\right) = F_5 \end{aligned}\right\} \tag{2.2}$$

or written in the solved form of $\frac{\partial p}{\partial \xi}, \ldots, \frac{\partial w}{\partial \xi}$:

$$\left.\begin{aligned} &\frac{\partial p}{\partial \xi} = \frac{c^2[F_1 a - \rho(rF_2 + \alpha F_3 + \beta F_4)] + F_5 a}{a^2 - \tau^2 c^2} \\ &\frac{\partial \rho}{\partial \xi} = \frac{1}{c^2}\left[-\frac{F_5}{a} + \frac{\partial p}{\partial \xi}\right] \\ &\frac{\partial u}{\partial \xi} = \frac{1}{a}\left[F_2 - \frac{r}{\rho}\frac{\partial p}{\partial \xi}\right] \\ &\frac{\partial v}{\partial \xi} = \frac{1}{a}\left[F_3 - \frac{\alpha}{\rho}\frac{\partial p}{\partial \xi}\right] \\ &\frac{\partial w}{\partial \xi} = \frac{1}{a}\left[F_4 - \frac{\beta}{\rho}\frac{\partial p}{\partial \xi}\right] \end{aligned}\right\} \tag{2.3}$$

where

$$a = ur + v\alpha + w\beta$$
$$\tau^2 = r^2 + \alpha^2 + \beta^2$$

$$F_1 = -\varepsilon\left\{\nu\frac{\partial\rho}{\partial\theta} + \frac{\omega}{\sin\theta}\frac{\partial\rho}{\partial\varphi} + \rho\left[2u + \frac{\partial v}{\partial\theta} + \frac{1}{\sin\theta}\left(v\cos\theta + \frac{\partial w}{\partial\varphi}\right)\right]\right\}$$

$$F_2 = -\varepsilon\left[\nu\frac{\partial u}{\partial\theta} + \frac{\omega}{\sin\theta}\frac{\partial u}{\partial\varphi} + (v^2 + w^2)\right]$$

$$F_3 = -\varepsilon\left[\nu\left(\frac{\partial v}{\partial\theta} + u\right) + \frac{\omega}{\sin\theta}\left(\frac{\partial v}{\partial\varphi} - \cos\theta w\right) + \frac{1}{\rho}\frac{\partial p}{\partial\theta}\right]$$

$$F_4 = -\varepsilon\left[\nu\frac{\partial w}{\partial\theta} + uw + \frac{\omega}{\sin\theta}\left(\frac{\partial w}{\partial\varphi} + v\cos\theta\right) + \frac{1}{\rho\sin\theta}\frac{\partial p}{\partial\varphi}\right]$$

$$F_5 = -\varepsilon\left[\nu\left(\frac{\partial\rho}{\partial\theta} - c^2\frac{\partial\rho}{\partial\vartheta}\right) + \frac{\omega}{\sin\theta}\left(\frac{\partial\rho}{\partial\varphi} - c^2\frac{\partial\rho}{\partial\varphi}\right)\right]$$

2.2 BOUNDARY CONDITIONS

(1) Shock wave conditions

Based on the shock wave, they must satisfy the shock wave relationship

$$\left.\begin{aligned}
&h + \frac{V_n^2}{2} = h_\infty + \frac{V_{n\infty}^2}{2}\\
&p + \rho V_n^2 = p_\infty + \rho_\infty V_{n\infty}^2\\
&u = u_\infty - \left(1 - \frac{\rho_\infty}{\rho}\right)n_1 V_{n\infty}\\
&v = v_\infty - \left(1 - \frac{\rho_\infty}{\rho}\right)n_2 V_{n\infty}\\
&w = w_\infty - \left(1 - \frac{\rho_\infty}{\rho}\right)n_3 V_{n\infty}
\end{aligned}\right\} \quad (2.4)$$

where quantities with subscript ∞ represent wave-front quantities, quantities without subscripts represent wave-tail quantities, V_n represents the projection of velocity in the direction of the shock wave normal, h is enthalpy, and (n_1, n_2, n_3) are the respective directional cosines of the shock wave normal, i.e.,

$$\begin{pmatrix} n_1\\ n_2\\ n_3\end{pmatrix} = \frac{1}{\sqrt{1 + \left(\frac{F_\theta}{r}\right)^2 + \left(\frac{F_\varphi}{r\sin\theta}\right)^2}} \times \begin{pmatrix} 1\\ -\frac{F_\theta}{r}\\ -\frac{F_\varphi}{r\sin\theta}\end{pmatrix}$$

(2) Object surface conditions

At the object surface they must satisfy normal velocity for zero conditions, i.e.,

$$q - uG - vG_0 - w\frac{G_0}{\sin\theta} = 0 \quad (2.5)$$

3. NUMERICAL SOLUTION

In order to carry out numerical solution, we introduced a number of rays in the solution region. For example, in the θ direction we introduced some coordinate planes with $\theta = \theta_i$ = const, in the φ direction we introduced some coordinate planes with $\varphi = \varphi_i$ = const and took the intersection lines of these coordinate planes as the rays. For fixed ξ, we used the value of the flow parameter based on the ray as the nodal point value to form an interpolation polynomial and thus were able to correspondingly determine the partial derivatives for θ and φ. Letting equation (2.3) be established on the basis of the rays will lead to a set of ordinary differential equations and the corresponding boundary value problems will become boundary value problems of a set of ordinary differential equations. For this we converted the boundary value problems into initial value problems and found the solution by iteration, i.e., given the shock wave form, we determined the flow parameters of the wave tail from shock wave conditions (2.4) and using these as the initial values, integrated the set of ordinary differential equations and then checked whether or not the object surface flow parameters thus obtained satisfied object surface conditions (2.5). If not, we then readjusted the shock wave form until the object surface conditions were satisfied. The usual methods, such as the four-step Runge-Kutta method, can be used for integrating the set of ordinary differential equations. Some of the actual treatments are described below.

3.1 Equations based on the $\theta = 0$ axis

Assuming a flow field with $\varphi = 0$, the π plane is symmetrical and the $\theta = 0$ axis is totally within the symmetrical plane. From equation

(2.2) it can be seen that since $\sin\theta$ appears in the denominator, equations with $\theta = 0$ must also be treated. Let $v^* = v(\xi, 0, 0)$, and it is evident that $v(\xi, 0, \varphi) = v^*(\xi)\cos\varphi$, $w(\xi, 0, \varphi) = -v^*(\xi)\sin\varphi$, $u(\xi, 0, \varphi) = u(\xi, 0, 0)$, $\rho(\xi, 0, \varphi) = \rho(\xi, 0, 0)$, $\rho(\xi, 0, \varphi) = \rho(\xi, 0, 0)$. We used Lobida's law for the percentage terms appearing in equation (2.2) and were easily able to obtain an equation based on $\theta = 0$. In principle, it is well to select equations based on a φ plane, but due to errors in numerical calculation, for different φ, the results obtained can be different. To eliminate such differences we integrated these equations for φ from 0 to π and obtained the desired equations. For example, after multiplying the third equation in (2.2) by $\cos\varphi$, and subtracting the fourth equation multiplied by $\sin\varphi$, we then carried out integration, and since

$$\int_0^\pi a\left(\frac{\partial v}{\partial \xi}\cos\varphi - \frac{\partial w}{\partial \xi}\sin\varphi\right)d\varphi = \int_0^\pi (ru + av \quad \beta w)\frac{\partial v^*}{\partial \xi}\,d\varphi = a^*\frac{\partial v^*}{\partial \xi}$$

$$\frac{1}{\rho}\int_0^\pi (a\cos\varphi - a_1\sin\varphi)\frac{\partial \rho}{\partial \xi}\,d\varphi = \frac{a^*}{\rho}\frac{\partial \rho}{\partial \xi}$$

$$\frac{1}{\pi}\int_0^\pi (F_1\cos\varphi - F_2\sin\varphi)d\varphi = -\frac{2\varepsilon}{\pi}\left\{\int_0^\pi\left[v^*\left(\frac{\partial v}{\partial\theta}\cos^2\varphi - \frac{\partial w}{\partial\theta}\sin\varphi\cos\varphi\right)\right.\right.$$

$$\left.\left. + \frac{1}{\rho}\frac{\partial \rho}{\partial\theta}\cos\varphi\right]d\varphi + \frac{\pi}{2}uv^*\right\} - F_1^*$$

consequently, we can obtain

$$a^*\frac{\partial v^*}{\partial \xi} + \frac{a^*}{\rho}\frac{\partial \rho}{\partial \xi} = F_1^*$$

similarly, we can obtain

$$a^*\frac{\partial u}{\partial \xi} + \frac{r}{\rho}\frac{\partial \rho}{\partial \xi} = F_2^*$$

$$a^*\frac{\partial \rho}{\partial \xi} + \rho\left(\frac{\partial u}{\partial \xi} + a^*\frac{\partial v^*}{\partial \xi}\right) = F_3^*$$

$$a^*\left(\frac{\partial \rho}{\partial \xi} - c^2\frac{\partial \rho}{\partial \xi}\right) = F_4^*$$

written in the form of $\frac{\partial \rho}{\partial \xi}, \cdots, \frac{\partial v^*}{\partial \xi}$, it is easy to obtain the desired equations

$$\left.\begin{aligned}
\frac{\partial \rho}{\partial \xi} &= \frac{c^2[F_1^* a^* - \rho(rF_2^* + a^*F_3^*)] + a^*F_4^*}{a^{*2} - r^{*2}c^2}\\
\frac{\partial \rho}{\partial \xi} &= \frac{1}{c^2}\left[-\frac{F_4^*}{a^*} + \frac{\partial \rho}{\partial \xi}\right]\\
\frac{\partial u}{\partial \xi} &= \frac{1}{a^*}\left[F_2^* - \frac{r}{\rho}\frac{\partial \rho}{\partial \xi}\right]\\
\frac{\partial v^*}{\partial \xi} &= \frac{1}{a^*}\left[F_1^* - \frac{a^*}{\rho}\frac{\partial \rho}{\partial \xi}\right]
\end{aligned}\right\} \qquad (2.6)$$

where

$$a^0 = \frac{2}{\pi}\int_0^{\pi} u\cos\varphi d\varphi$$

$$a^0 = ru + a^0 v^0$$

$$\tau^{0j} = r^j + a^{0j}$$

$$F_1^0 = -\frac{2\varepsilon}{\pi}\left\{v^0\int_0^{\pi}\frac{\partial\rho}{\partial\theta}\cos\varphi d\varphi + \rho\int_0^{\pi}\frac{\partial v}{\partial\theta}d\varphi + \rho u\pi\right\}$$

$$F_2^0 = -\frac{2\varepsilon}{\pi}\left\{v^0\int_0^{\pi}\frac{\partial u}{\partial\theta}\cos\varphi d\varphi - \frac{\pi}{2}v^{02}\right\}$$

$$F_3^0 = -\frac{2\varepsilon}{\pi}\left\{\int_0^{\pi}\left[v^0\left(\frac{\partial v}{\partial\theta}\cos\varphi - \frac{\partial w}{\partial\theta}\sin\varphi\cos\varphi\right) + \frac{1}{\rho}\frac{\partial p}{\partial\theta}\cos\varphi\right]d\varphi + \frac{\pi}{2}uv^0\right\}$$

$$F_4^0 = -\frac{2\varepsilon}{\pi}v^0\int_0^{\pi}\left(\frac{\partial r}{\partial\theta} - \varepsilon^j\frac{\partial\rho}{\partial\theta}\right)\cos\varphi d\varphi$$

3.2 Interpolation polynomials

Since it is assumed that the flow field for $\varphi = 0$ and the x plane are symmetrical, therefore a solution is required only between $0 \leq \varphi \leq \pi$. We introduced k + 1 half-planes between 0 and π. At the same time, n + 1 cones are formed, $\theta = \theta_k$ = const ($\theta_0 = 0$), $k = 0, 1, \ldots, n$. They intersect half-planes $\varphi = \varphi_i$ and $\varphi = \varphi_i + \pi$ forming (2n + 1) rays. Note symmetry of flow parameters and that those for $\varphi = \pi - \varphi_i$ are equal to those for $\varphi = \varphi_i + \pi$, or differ in sign. Consequently, for a fixed ξ, the values for 2n + 1 rays at $\varphi = \varphi_i$ and $\varphi = \pi - \varphi_i$ can be used to form θ interpolation polynomials of the 2n-th degree:

$$g = \sum_{i=0}^{2n} a_i\theta^i \qquad (2.7)$$

g represents a flow parameter. To save time in calculation, we did not precalculate coefficient a_i, but used the following algorithm: since the interpolating function and its derivative can both be represented as a linear combination of functional values for the interpolation nodal point, and since the linear combination coefficient is related to both the position of the interpolation nodal point and the position of the interpolation point, therefore, once these nodal points and interpolation points are fixed, the coefficients can be determined and when the function and derivative values of the various points must be calculated, it is only necessary that the functional values for these coefficients and nodal points be scalar products.

Taking equation (2.7) as an example, assume that the nodal point is $\theta m (m = 0, 1, \ldots, 2n)$. We must calculate $g(\theta)$ at some interpolation point θ. Since at the nodal point there is the condition

$$\sum_{i=0}^{2n} a_i \theta_m^i = g_m \quad (m = 0, 1, \cdots, 2n)$$

$g_m = g(\theta_m)$. Or written in the form of a matrix:

$$Ma = g$$

where

$$M = \begin{pmatrix} 1 & \theta_0 & \theta_0^2 \cdots\cdots\cdots & \theta_0^{2n} \\ 1 & \theta_1 \cdots\cdots\cdots\cdots & & \theta_1^{2n} \\ \cdots\cdots\cdots\cdots\cdots\cdots & & & \\ 1 & \theta_{2n} \cdots\cdots\cdots\cdots & & \theta_{2n}^{2n} \end{pmatrix}$$

$$a = \begin{pmatrix} a_0 \\ a_1 \\ \vdots \\ a_{2n} \end{pmatrix} \quad g = \begin{pmatrix} g_0 \\ g_1 \\ \vdots \\ g_{2n} \end{pmatrix}$$

Therefore, we have

$$a = M^{-1}g$$

Thus, the equation for $g(\theta)$ can be considered as

$$g(\theta) = d^* \cdot a$$

rewritten as

$$\begin{aligned} g(\theta) &= d^* \cdot (M^{-1}g) \\ &= (M^{-1*}d)^* \cdot g \\ &= b^* \cdot g \end{aligned} \qquad (2.8)$$

where $b = M^{-1*}d$, and $d^* = (1, \theta, \ldots, \theta^{2n})$. It is evident that when the nodal points and interpolation points are fixed, M^* and d can both be determined and thus we will also be able to obtain b. Likewise, since

$$\begin{aligned} g_\theta'(\theta) &= \sum_{i=0}^{2n} a_i i(\eta)^{i-1} \\ &= d_1^* \cdot a \\ &= (M^{*-1}d_1)^* \cdot g \end{aligned}$$

where $d_1^* = (0, 1, 2\theta, \ldots, 2n\theta^{2n-1})$, the prime (') represents a derivative of θ and therefore we consider the derivative can be similarly treated.

With respect to θ, when θ is fixed, we use the value where it intersects the k + 1 half-plane to construct the trigonometric interpolation polynomial for θ. The method mentioned above is also used in calculation. For even functions we take

$$g = \sum_{i=0}^{k} a_i \cos^i \varphi$$

therefore

$$g_i' = (M^{0-1} d_i)^0 \cdot g$$

we now have

$$M^0 = \begin{pmatrix} 1 & 1 & \cdots & 1 \\ \cos\varphi_0 & \cos\varphi_1 & \cdots & \cos\varphi_k \\ \vdots & \vdots & \cdots & \vdots \\ \cos^k\varphi_0 & \cos^k\varphi_1 \cdots & \cos^k\varphi_k & \end{pmatrix}$$

$$d_i^0 = (0, -\sin\varphi, \cdots, -k\sin\varphi\cos^{k-1}\varphi)$$

$$g^0 = (g_0, g_1, \cdots, g_k)$$

for $\frac{1}{\pi}\int_0^{\pi} g\,d\varphi$, $\frac{1}{\pi}\int_0^{\pi} g\cos\varphi\,d\varphi$ we can also write similar expressions which have not been enumerated. For odd functions we take

$$g = \sum_{i=0}^{k-1} a_i \cos^i\varphi \sin\varphi$$

hence

$$g_i' = (M^{0-1} d_i)^0 g$$

Now

$$M^0 = \begin{pmatrix} \sin\varphi_1 & \sin\varphi_2 \cdots\cdots\cdots\cdots \sin\varphi_{k-1} \\ \sin\varphi_1\cos\varphi_1 & \vdots & \vdots \\ \vdots & \vdots & \vdots \\ \sin\varphi_1\cos^{k-2}\varphi_1 & \sin\varphi_1\cos^{k-2}\varphi_2 \cdots & \sin\varphi_{k-1}\cos^{k-2}\varphi_{k-1} \end{pmatrix}$$

$$d_i^0 = (\cos\varphi, -\sin^2\varphi + \cos^2\varphi, \cdots, (k-2)\cos^{k-1}\varphi\sin^2\varphi + \cos^{k-1}\varphi)$$

In addition to the method described above, we also used the following method to construct interpolation polynomials. For even functions of φ we take

$$g(\xi) = \sum_{i=0}^{n} \sum_{j=0}^{k} g_{ij}(\xi)\theta^i \cos^j\varphi$$

for odd functions we take

$$w(\xi) = \left(\sum_{i=0}^{n} \sum_{j=0}^{k} w_{ij}(\xi)\theta^i \cos^j\varphi\right) \sin\varphi$$

In order to bring the function and its derivative for θ to a single value at $\theta = 0$, we must add the appropriate conditions to the polynomial. Now to explain such conditions.

For example, for a shock wave form of $r = F(\theta, \varphi)$, when $\theta = 0$, we naturally require that it be independent of θ. This merely requires that $F_{0j} = 0$ when $j \neq 0$. At the same time, in order to ensure that the normal has a definite direction, when $\theta = 0$ the direction of the normal under spherical coordinates should have a form such as this: $(a, b\cos\varphi, -b\sin\varphi)$, where a and b are arbitrary constants. This requires that $F_{1j} = 0\ (j \neq 1)$. Therefore, for F the polynomial should be

$$F(\theta, \varphi) = F_{00} + F_{11}\theta\cos\varphi + \sum_{i=1}^{n}\sum_{j=0}^{k} F_{ij}\theta^i\cos^j\varphi \qquad (2.9)$$

It is evident that u, p, ρ should also take the same form as F. The above conclusion and the v and w forms can still be obtained by the following means. We let

$$g = g_{00}(\xi) + \sum_{i=1}^{n}\sum_{j=0}^{k} g_{ij}(\xi)\theta^i\cos^j\varphi$$

$$v = v_{11}(\xi)\cos\varphi + \sum_{i=1}^{n}\sum_{j=0}^{k} v_{ij}(\xi)\theta^i\cos^j\varphi$$

$$w = -v_{11}(\xi)\sin\varphi + \left(\sum_{i=1}^{n}\sum_{j=0}^{k} w_{ij}(\xi)\theta^i\cos^j\varphi\right)\sin\varphi$$

where g can represent p, ρ, u, F, and the characteristics $v(\xi, 0, \varphi) = A\cos\varphi$, $w(\xi, 0, \varphi) = -A\sin\varphi$, were used, and therefore we have $v_{ij} = 0\ (j \neq 1)$, $w_{ij} = 0\ (j \neq 0)$, $v_{11} = -w_{00}$. Entering the above formula into equation (2.2), notice that

$$\frac{\partial}{\partial\theta}G(0, \varphi) = G_\theta(0, 0)\cos\varphi,$$

$$\frac{G_\varphi}{\sin\theta}\bigg|_{\theta=0} = -G_\theta(0, 0)\sin\varphi.$$

(where we assume that the object surface is at $\varphi = 0$ and the π plane is symmetrical. Therefore, when $\theta \to 0$, we can obtain

$$a_0\frac{d\rho_{00}}{d\xi} + r_0\rho_{00}\frac{du_{00}}{d\xi} - \rho_{00}[G_{01} + \xi(F_{11} - G_{00})]\frac{dv_{01}}{d\xi} = \lim_{\theta\to 0} F_1$$

$$a_0\frac{du_{00}}{d\xi} + \frac{r_0}{\rho_{00}}\frac{dp_{00}}{d\xi} = \lim_{\theta\to 0} F_2$$

$$\left(a_0\frac{dv_{01}}{d\xi} - \frac{G_{01} + \xi(F_{11} - G_{00})}{\rho_{00}}\frac{dp_{00}}{d\xi}\right)\cos\varphi = \lim_{\theta\to 0} F_3$$

$$-\left(a_0\frac{dv_{01}}{d\xi} - \frac{G_{01} + \xi(F_{11} - G_{00})}{\rho_{00}}\frac{dp_{00}}{d\xi}\right)\sin\varphi = \lim_{\theta\to 0} F_4$$

$$a_0\left(\frac{dp_{00}}{d\xi} - c_0^2\frac{d\rho_{00}}{d\xi}\right) = \lim_{\theta\to 0} F_5$$

where

$$a_\xi = u_\infty r_\xi - v_{01}[G_\theta + \xi(F_{11} - G_\theta)]$$
$$r_\xi = G(0,0) + \xi[F_\infty - G(0,0)]$$
$$G_\infty = \frac{\partial}{\partial\theta} G(0,0)$$
$$c_0^2 = \frac{\gamma p_\infty}{\rho_\infty}$$

The right side of the above formula is written as a polynomial of $\cos\varphi$ (or multiplied by $\sin\varphi$) and using the linear independence of $1, \cos\varphi, \cdots, \cos^k\varphi$ it can be easily deduced that g should take the form of equation (2.9) and v and w should take the form

$$v = v_{01}\cos\psi + v_{10}\theta + v_{11}\theta\cos^2\varphi + \sum_{i=2}^{\infty}\sum_{j=0}^{i} v_{ij}\theta^j\cos^i\varphi$$

$$w = -v_{01}\sin\varphi - v_{11}\theta\cos\varphi\sin\varphi + \left(\sum_{i=2}^{\infty}\sum_{j=0}^{i} w_{ij}\theta^j\cos^i\varphi\right)\sin\varphi$$

At the same time, we have also obtained an equation based on $\theta = 0$:

$$\left.\begin{aligned}
&a_\xi\frac{dp_\infty}{d\xi} + r_0\rho_\infty\frac{du_\infty}{d\xi} - \rho_\infty[G_\theta + \xi(F_{11} - G_\theta)]\frac{dv_{01}}{d\xi} \\
&\quad = -(F_\infty - G(0,0))[v_{01}\rho_{11} + \rho_\infty(v_{12} + 2v_{10} + 2u_\infty)] \\
&a_\xi\frac{du_\infty}{d\xi} + \frac{r_0}{\rho_\infty}\frac{dp_\infty}{d\xi} = -(F_\infty - G(0,0))v_{01}(u_{11} - v_{01}) \\
&a_\xi\frac{dv_{01}}{d\xi} - \frac{G_\theta + \xi(F_{11} - G_\infty)}{\rho_\infty}\frac{dp_\infty}{d\xi} \\
&\quad = -(F_\infty - G(0,0))\left[v_{01}(v_{10} + v_{12} + u_\infty) + \frac{p_{11}}{\rho_\infty}\right] \\
&a_\xi\left(\frac{dp_\infty}{d\xi} - c_0^2\frac{d\rho_\infty}{d\xi}\right) = -(F_\infty - G(0,0))\,v_{01}\left(p_{11} - \frac{\gamma p_\infty}{\rho_\infty}\rho_{11}\right)
\end{aligned}\right\} \quad (2.10)$$

3.3 Iteration methods

Just as mentioned in the beginning of this section, we solved the boundary value problems by iteration. In fact, this can also be understood by solving the problem of a set of nonlinear transcendental equations, i.e., selecting an F_j set (representing the shock wave form at the j-th ray), we use

$$q_j(F_1, \cdots, F_m) = 0 \quad (j = 1, 2, \cdots, m)$$

where $q_1 = 0$, i.e., boundary condition (2.5). We used the Newton method, i.e., the change in F_j value, δF_j, satisfies the following equation:

$$\sum_{i=0}^{m} \frac{\partial q_j}{\partial F_i} \delta F_i = -q_j \quad (j = 1, \cdots, m)$$

Normally, the partial derivative $\frac{\partial q_j}{\partial F_i}$ is incapable of being expressed in analytical form, therefore we used the numerical method, i.e.,

$$\frac{\partial q_j}{\partial F_i} = \frac{q(F_1, \cdots, F_{i-1}, F_i + \Delta F_i, F_{i+1}, \cdots, F_m) - S_j(F_1, \cdots, F_m)}{\Delta F_i}$$

Using this method, each time we iterate, we then must integrate m + 1 times, hence an extraordinary expenditure of machine time. To save time, the simplified Newton method can be used, but since $\frac{\partial q_j}{\partial F_i}$ is probably not very exact, the convergence rate may be relatively slow. To make $\frac{\partial q_j}{\partial F_i}$ a little more accurate, but without increasing the calculated value very much, we suggest the following method. Let Q represent a vector consisting of q_1, ..., q_m, and let R represent a vector consisting of F_1, ..., F_m. The Q to R guidepost [sic] was expressed as Q'. Given that $Q(R_0) = Q_0$ and m points R_1, ..., R_m are located outside the vicinity of R_0 and it is known that $Q(R_i) = Q_i (i = 1, \ldots, m)$, and if $R_0 - R_i (i = 1, 2, \ldots, m)$ is linearly independent, then Q_0' can be approximated from R_i and Q_i. In fact, since

$$Q_i \approx Q_i + Q_i'(R_i - R_0) \quad (i = 1, 2, \cdots, m)$$

we therefore have

$$(Q_1 - Q_0, \cdots, Q_m - Q_0) \approx Q_0'(R_1 - R_0, \cdots, R_m - R_0)$$

thus we have

$$Q_0' \approx (Q_1 - Q_0, \cdots, Q_m - Q_0)(R_1 - R_0, \cdots, R_m - R_0)^{-1}$$

and therefore can obtain the iteration formula

$$R_{n+1} = R_n - (R_{n-m} - R_n, \cdots, R_{n-1} - R_n)(Q_{n-m} - Q_n, \cdots, Q_{n-1} - Q_n)^{-1} Q_n \quad (2.11)$$
$$n = m + 1, \cdots$$

It is obvious that using the above formula to carry out iteration, first to find Q_1, ..., Q_{m+1} from R_1, ..., R_{m+1} requires integration m + 1 times, but subsequent iteration only requires integration one time. Now a simple estimate for convergence rate. It is obvious that when

$$\bar{R}_{n+1} = (R_1 - R_{n+1}, \cdots, R_m - R_{n+1}) = \Delta F \cdot E$$

equation (2.11) is a differencing Newton formula in which E is the unit matrix and ΔF is a scalar quantity. Since we now have

$$\tilde{Q}_{n-1} = (Q_1 - Q_{n-1}, \cdots, Q_n - Q_{n-1}) = Q_{n-1}\tilde{R}_{n-1} + o(\Delta F^2)$$

therefore we have

$$Q_{n-1}^{-1} = \tilde{R}_{n-1}\tilde{Q}_{n-1}^{-1} + o(\Delta F^2)\tilde{Q}_{n-1}^{-1} = \tilde{R}_{n-1}\tilde{Q}_{n-1}^{-1} + o(\Delta F)$$

consequently for the differencing Newton formula we have the estimating formula

$$\begin{aligned} R^* - R_{n-1} &= R^* - R_{n-1} + \tilde{R}_{n-1}\tilde{Q}_{n-1}^{-1}Q_{n-1} \\ &= R^* - R_{n-1} + Q_{n-1}^{-1}Q_{n-1} + (\tilde{R}_{n-1}\tilde{Q}_{n-1}^{-1} - Q_{n-1}^{-1})Q_{n-1} \\ &= o(\|R^* - R_{n-1}\|^2) + o(\Delta F\|Q_{n-1}\|) \end{aligned}$$

or written as

$$\|R^* - R_n\| \leqslant A\|R^* - R_{n-1}\|^2 + B\Delta F\|Q_{n-1}\| \quad (n = 1, 2, \cdots)$$

where R* represents the genuine solution, $\|\ \|$ represents a modulus, and A and B are both appropriate constants. Likewise, for a simplified differencing Newton method there is the estimating formula

$$\|R^* - R_n\| \leqslant A\|R^* - R_{n-1}\| + B\Delta F\|Q_{n-1}\| + C\|R_{m+1} - R_{n-1}\|\|Q_{n-1}\|$$
$$(n = m + 2, \cdots)$$

For the method we proposed there is the estimating formula

$$\|R^* - R_n\| \leqslant A\|R^* - R_{n-1}\| + D\|\tilde{Q}_{n-1}^{-1}\| \sup_{1<i<n} \|R_{n-1} - R_{n-1-i}\|\|Q_{n-1}\|$$

where A, B, C, and D are all constants.

It is not difficult to see that when ΔF is on the same order or smaller than $\|R^* - R_{n-1}\|$, the differencing Newton method basically maintains the convergence rate of the Newton method. But, generally $\|R_{m+1} - R_{n-1}\|$ increases as n increases, and therefore the convergence rate of the simplified Newton method is relatively slow. Since $\tilde{Q}_{n-1}^{-1}\| \sup_{1<i<n} \|R_{n-1} - R_{n-1-i}\| = o(1)$, and $\sup_{1<i<n} \|R_{n-1} - R_{n-1-i}\|$ decrease with an increase in n, therefore the method we propose can converge somewhat faster than the simplified Newton method. Actual calculations have confirmed this point.

3.4. Initial shock wave selection and object surface value extrapolation

When using the method mentioned above to conduct iteration, whether the shock wave is well selected or not is rather important for

calculating whether or not it will be successfully carried out. For this reason, we used the results already obtained on the basis of step-by-step interim measures of certain parameters. For example, when we want to consider the results of flow under a certain angle of attack η^*, angle of attack η can be selected as a parameter. After the results of η_0 have been calculated (for example $\eta_0 = 0°$), then we can regard it as the initial value of $\eta_0 + \Delta\eta$, and after calculating the results of $\eta_0 + \Delta\eta$, we can then use the results of η_0, $\eta_0 + \Delta\eta$ and use linear interpolation to determine the initial value of $\eta_0 + 2\Delta\eta$. And so forth and so on, until the results of η^* have been determined. As to first calculation of the required initial shock wave form, this can be accomplished by using available results.

It can be seen from equation (2.3) that $a = 0$ on the object surface and therefore integration is not carried out up to the object surface. In order to determine the object surface value, we used the extrapolation method, i.e., integration is carried out until a certain ξ^* is reached (for example $\xi^* = 0.1$), then using the ξ value of several adjacent points we extrapolate the object surface value, for example, using the values $\xi = 0.3, 0.2, 0.1$ is regarded as two-step interpolation. It should be mentioned in passing that if another form of calculation is used, for example the implicit form, to carry out integration, extrapolation can be completely avoided. For conditions of axial symmetry, we designed a mode and carried out the calculations and the results indicate that it was a success. It is not described in any detail here.

4. RESULTS OF CALCULATIONS

We used the methods described above to conduct extensive calculations on axisymmetric and three-dimensional flow about blunt-nosed bodies. The shapes of the calculated objects were ellipsoids and nearly disc-shaped objects with various axial ratios (the objects are represented by the equation $z^n + (x^2+y^2)^{n/2} = 1^n$, and $n \geqslant 2$). The Mach number range of the oncoming flow was $1.5 \leqslant M_\infty \leqslant \infty$. For

conditions of axial symmetry, in addition to frozen gas with $\gamma = 1.4$, we also conducted calculations for equilibrium air and non-equilibrium air. The method described in [12] was used to calculate the thermodynamic functions of equilibrium air. See our other articles for non-equilibrium gases. The accuracy of the computational results was checked in various ways. One was the carrying out of the computations themselves, for example, the use of different numbers of rays and different integral step lengths and conducting checks on certain relationships which the flow field must satisfy, such as the condition of total conservation of energy. Another was making comparisons of results obtained from experiments and from other methods such as the integral relationship method. All the checks indicated that the accuracy of the computed results was quite satisfactory. Part of the computed results is given below.

Figure 1 shows the shape of shock waves and sonic speed lines for the flow of frozen gases about a sphere at different M_∞ numbers. It is evident from the figure that the sonic speed line forms appear in two types: At $M > 3$, the limiting characteristic line is the second family of characteristic lines to reach the object surface sonic speed point; and at $M < 3$, the limiting characteristic line is made up of the first family of characteristic lines in contact with the sonic speed line (generated by the object surface) and the second family of characteristic lines (generated by the shock wave).

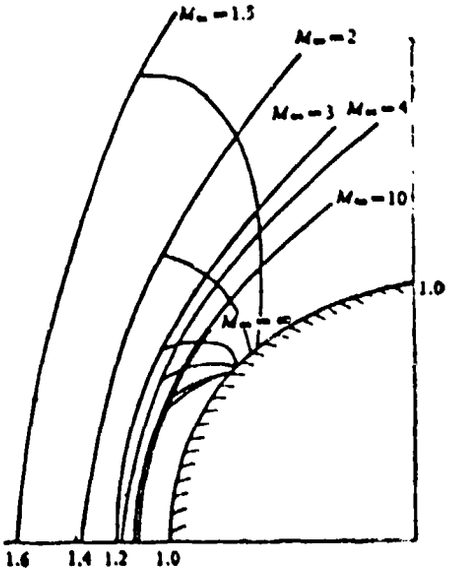

Fig. 1. The shock wave and sonic speed line shapes for the flow of frozen gases about a sphere

Figure 2 shows the object surface pressure distribution for frozen gas flow about a sphere.

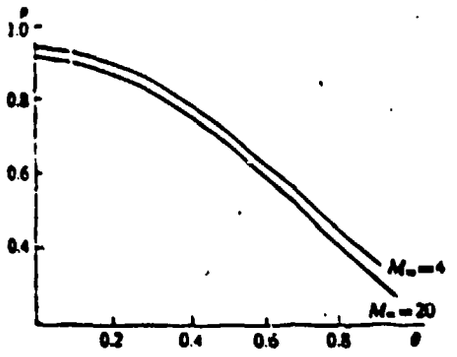

Fig. 2. Distribution of pressures over the object surface

Figure 3 shows shock wave shape and sonic speed line location for different objects, $M_\infty = 3$, $\gamma = 1.4$. For a very blunt body, for example $n > 20$, the position of the shock wave will generally remain unchanged. With a decrease in the radius of curvature of the object surface in the vicinity of the sonic speed points, for a fixed M_∞ number, beginning with a certain curvature the sonic speed line will exhibit an inflection point.

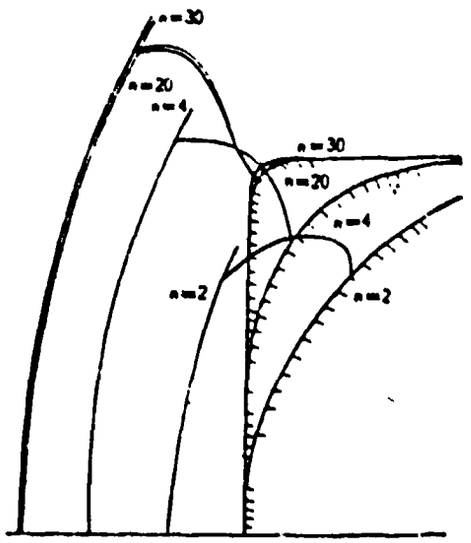

Fig. 3 Shock wave locations and sonic speed line shapes ($M_\infty = 3$)

Figure 4 present equilibrium gas flow about a sphere and the shock wave locations and sonic speed line shapes at different M_∞ numbers.

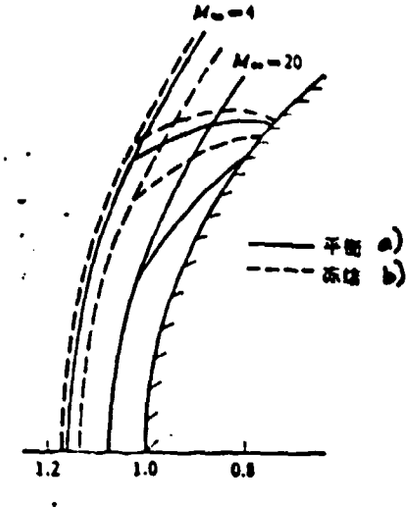

Fig. 4. Shock wave and sonic speed line shapes for the flow of equilibrium gas about a sphere

KEY: a) equilibrium; b) frozen

The flow conditions are: $M_\infty = 4$, $p_\infty = 0.87 \times 10^3$ dynes/cm^2, $\rho_\infty = 0.95 \times 10^{-6}$ g/cm^3 and $M_\infty = 20$, $p_\infty = 0.122 \times 10^6$ dynes/cm^2, $\rho_\infty = 0.192 \times 10^{-3}$ g/cm^3. It is evident from the figure that dissociation causes the shock wave location and sonic speed line to markedly differ from that of frozen gas with $\gamma = 1.4$. The shock wave draws very near to the object surface.

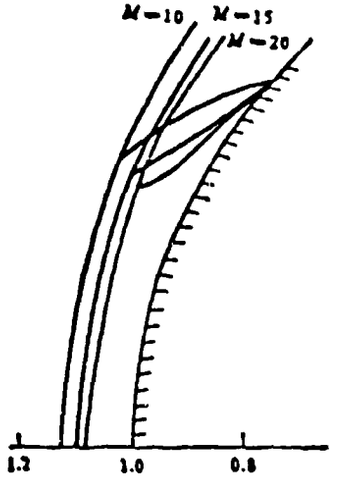

Fig. 5. Shock wave and sonic speed line shapes for the flow of non-equilibium gas about a sphere

Figure 5 shows shock wave location and sonic speed line sha for the flow of non-equilibrium gas about a sphere. The conditions of the oncoming flow are: $p_\infty = 0.947 \times 10^3$ dynes/cm^2, $\rho_\infty = 0.123 \times 10^{-5}$ g/cm^3, R = 5 cm. It should be noted that the $M_\infty = 20$ sonic speed line has a peculiar shape at the shock wave.

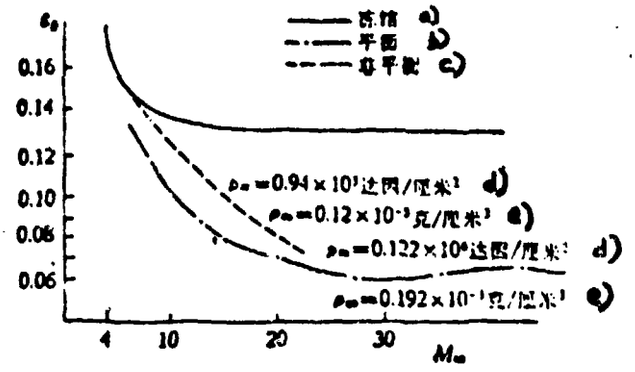

Fig. 6. Stagnation point shock wave detachment distance along with changes in M_∞

KEY: a) frozen; b) equilibrium; c) non-equilibrium; d) dynes/cm^2; e) g/cm^3.

Figure 6 shows the relationship between the M_∞ number and the detachment distance of the stagnation point. For frozen flow, with $M > 10$, it basically remains unchanged. For equilibrium air, with an increase in M_∞, a change in detachment distance occurs without monotonicity.

When calculating axisymmetric flows normally five rays are used.

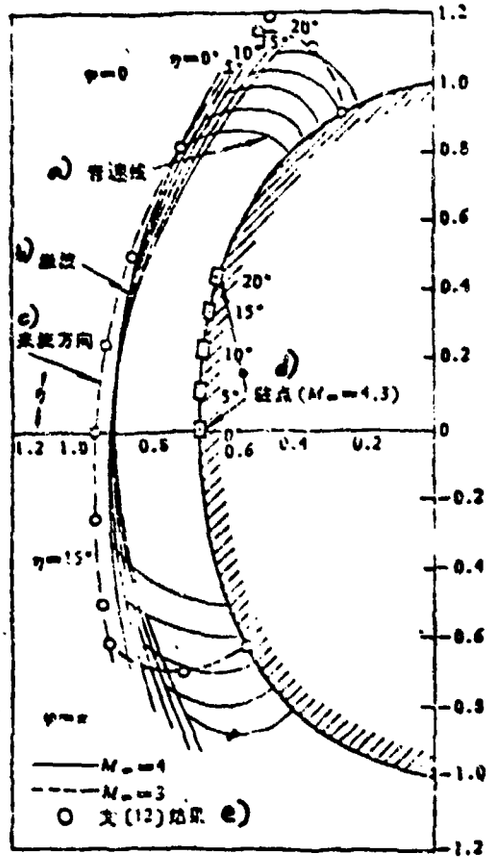

Fig. 7. Shock wave shapes and sonic speed lines within a symmetrical plane along with changes in angle of attack

KEY: a) sonic speed line; b) shock wave; c) direction of oncoming flow; d) stagnation point (M_∞ = 4, 3); e) Results from [12]

Figure 7 presents the flow about an ellipsoid with $\delta = 1.5$ and the shock waves and sonic speed lines within a symmetrical plane at M_∞ = 3 and 4 along with changes in angle of attack η. Figure 9 presents the object surface pressure within a symmetrical plane along with changes in angle of attack. Figure 7 also presents the location of the stagnation points and, within the accuracy of the figure, the stagnation points for $M_\infty = 3$ and $M_\infty = 4$ duplicate each other. When the angle of attack changes, the stagnation point moves over the object surface at a nearly uniform rate. Figure 8 presents the shock waves and sonic speed lines within the $\varphi = \pi/2$ plane along with changes in angle of attack. In the figure it can be seen that changes in shock wave shape are slow, but the changes in sonic speed lines are relatively quick.

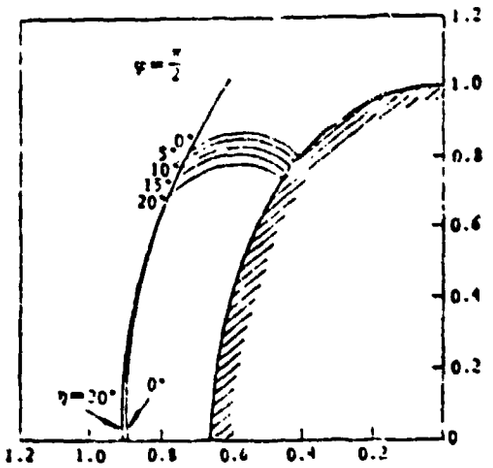

Fig. 8. Shock wave shapes and sonic speed lines with changes in angle of attack ($M_\infty = 4$, $\delta = 1.5$)

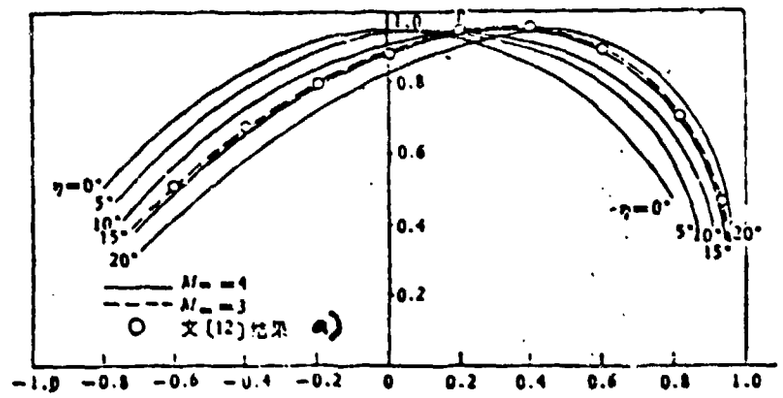

Fig. 9. Object surface pressure within a symmetrical plane along with changes in angle of attack ($\delta = 1.5$)

KEY: a) Results from [12]

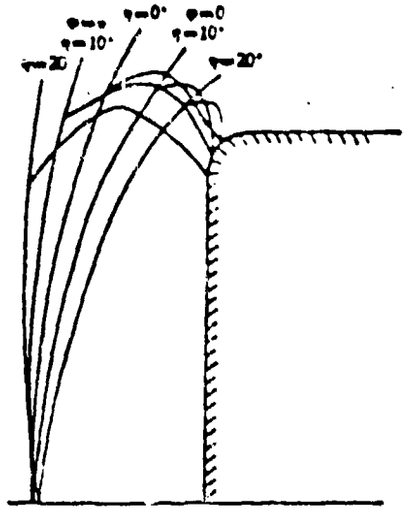

Fig. 10. Shock wave shapes and sonic speed lines on a symmetrical surface (M_∞ = 5.8, n = 20)

Figure 10 presents the flow about a disc-shaped object for M_∞ = 5.8 and n = 20 and the shock waves shapes and sonic speed line locations on a symmetrical plane at different angles of attack. Figure 11 presents the object surface pressure distribution within an axial [sic] plane.

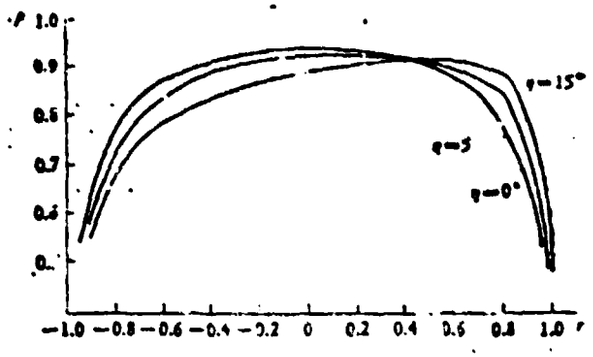

Fig. 11. Object surface pressure distribution within a symmetrical plane (M_∞ = 5.8, n = 20)

When calculating three-dimensional flow, we generally take four φ planes, and within each φ plane we take four rays. And because the axes are common, altogether we take 13 rays. The coordinate system z-axis extends into the symmetrical plane of the flow field and for convenience of calculation we usually use the included angle $\overline{\beta}$ between the flow field symmetrical plane and the body symmetrical axis (angle $\overline{\beta}$ = (0.5 - 0.6)η, and η is the angle of attack).

In regard to the question of whether or not maximum entropy value is reached on the object surface, it can be seen from our calculations that for certain types of objects, within a given range of error, maximum entropy is reached.

We employed several means to check the results of our calculations. We used different numbers of rays, for example, for axisymmetrical flows we conducted separate calculations using five rays and three rays and the results indicated an error of within 1%. We also employed different integral step lengths. For example, for flow about a sphere with $M_\infty = 6$ and $\gamma = 1.4$, from the shock wave to the object surface, integrals of 10 steps, 20 steps, and 80 steps. The relative error in the results obtained with 10 and 20 steps did not exceed 0.3% and between 20 to 80 steps, there was at least the same three significant digits. This also explains that we did not have to be overly concerned about rounding off error increases.

We made a comparison between the results for $M_\infty = 3$, $\delta = 1.5$, $\eta = 15^\circ$ and the results obtained by Telenin [16] and it can be seen from Figure 1 that they are exactly the same. For frozen flows about ellipsoids and spheres with $\delta = 1.5$, the results of our calculations agree with those obtained by Belotserkovskiy using the integral relationship method up to three significant digits.

We also conducted integral checks, i.e., we also checked the accuracy of integral equation

$$\iint_\sigma \rho \mathbf{u} \cdot d\sigma = 0$$

$$\iint_\sigma u_i \rho \mathbf{u} \cdot d\sigma + \iint_\sigma p x_i \cdot d\sigma = 0 \qquad (i = 1, 2, 3)$$

$$\iint_\sigma p\rho^{-1} \rho \mathbf{u} \cdot d\sigma = 0$$

where x_i represents the unit vector in the 3 axial directions under rectangular coordinates, u_i is the projection of velocity loss u in these three directions, σ is any curved surface which does not include the shock wave. See Table 1 for the results of integration for

$M_\infty = 4$, $\delta = 1.5$, $\eta = 10^\circ, 20^\circ$. Besides the total integral, Table 1 also gives the integral for the shock wave, for the object surface and for the cone. It can be seen from Table 1 that the calculated results are correct and that integrals for the shock wave and cone differ only in the third digit. Object surface conditions are also rather well satisfied, being on the order of 10^{-4}.

η	方程 (a)	激波面 (b)	物面 (c)	锥面 (d)	总和 (e)
10°	质量 (f)	−0.64327×2	0.00066×2	0.64513×2	0.00256×2
	x方向动量(g)	0.04595×2	−0.00731×2	−0.03849×2	0.00015×2
	y方向动量(h)	0	0	0	0
	z方向动量(j)	0.67039×2	−0.32282×2	−0.34862×2	−0.00105×2
	熵 (k)	−0.03789×2	0.00006×2	0.05809×2	0.00026×2
20°	质量 (f)	−0.63068×2	0.00054×2	0.63298×2	0.00284×2
	x方向动量(g)	0.09011×2	−0.01579×2	−0.07348×2	0.00035×2
	y方向动量(h)	0	0	0	0
	z方向动量(j)	0.65271×2	−0.30687×2	−0.34423×2	−0.00139×2
	熵 (k)	−0.05037×2	0.00008×2	0.05663×2	0.00033×2

Table 1. Integral checks $M_\infty = 4$, $\delta = 1.5$, $\bar{\beta} = 0.6\eta$

KEY: (a) equation; (b) shock wave surface; (c) object surface; (d) cone surface; (e) Total; (f) mass; (g) momentum in direction x; ion; (h) momentum in direction y; (j) momentum in direction z; (k) entropy

Furthermore, we calculated the total energy at all the nodal points and the entropy of each nodal point on the object surface. From Table 2 it can be seen that with $M_\infty = 4$, $\delta = 1.5$, when $\eta \leqslant 15^\circ$, the relative error of total energy is less than 1%. From Table 3 it can be seen that with $M_\infty = 4$, $\delta = 1.5$, and $\eta \leqslant 15^\circ$, the object surface entropy differs only by 1 at the third significant digit.

Table 2. Total energy difference

The exact value for $\frac{u^2+v^2+w^2}{2} + \frac{\gamma}{\gamma-1}\frac{p}{\rho}$ is 0.65625, at $M_\infty = 4$

η	a) 总能最大偏差	b) 相对误差
0°	0.0010	0.15%
5°	0.0019	0.30%
10°	0.0034	0.51%
15°	0.0051	0.76%
20°	0.0087	1.33%

KEY: (a) total energy maximum deviation; (b) relative error

Table 3. Entropy value of object surface nodal points ($\ln\rho - \gamma\ln\rho$)

When $M_\infty = 4$, $\delta = 1.5$, $\bar{\beta} = 0.6\eta$, $\eta = 0$, the exact value is -2.31904

φ \ η		0°	10°	20°
0°	0	-2.31903	-2.31537	-2.30611
11°	0	-2.31853	-2.31346	-2.30865
	$\frac{1}{3}\pi$		-2.31474	-2.31962
	$\frac{2}{3}\pi$		-2.31833	-2.31361
	π		-2.32091	-2.31858
22°	0	-2.31951	-2.32040	-2.31554
	$\frac{1}{3}\pi$		-2.31942	-2.32117
	$\frac{2}{3}\pi$		-2.31939	-2.31759
	π		-2.32077	-2.32111
33°	0	-2.31723	-2.31276	-2.30283
	$\frac{1}{3}\pi$		-2.31543	-2.31361
	$\frac{2}{3}\pi$		-2.31854	-2.31903
	π		-2.32045	-2.32421

In short, using the straight-line method to calculate flow about smooth bodies, the accuracy of the results is satisfactory.

Comrade Rui Weiming participated in part of the work, Comrade He Jiaomin gave us much assistance, and Comrade Feng Kang enthusiastically directed our work and for this we express our thanks to them.

Bibliography

[1] Telenin, G. F., Tinyakov, G. P., Method of calculating three-dimensional flow about bodies with detached shock waves. DAN USSR, 154, 5 (1964).

[2] Gilinskiy, S. M., Telenin, G. F., Tinyakov, G. P., Method of calculating supersonic flow about blunt bodies with detached shock waves. IAN USSR, OTN, Mekhanika i Mashinostroyeniye, 4 (1964).

[3] Glinskiy, S. M., Telenin, G. F., Supersonic flow about bodies of various shapes having detached shock waves. IAN USSR, OTN, Mekhanika i Mashinostroyeniye, 5 (1964).

[4] Glinskiy, S. M., Makarova, N. Ye., Calculation of supersonic flow about blunt bodies by an airstream taking into account equilibrium physical-chemical transformations. IAN USSR, MZhG, 1 (1966).

[5] Stulov, V. P., Telenin, G. F., Non-equilibrium flow of a supersonic airstream about a sphere. IAN USSR, Mekhanika, 1 (1965).

[6] Van Dyke, M. D., The supersonic blunt-body problem - Review and extension. J. A. S., 25, 8 (1958).

[7] Belotserkovskiy, O. M., Symmetrical flow of a supersonic stream of ideal and real gases about blunt bodies. Zh. VMMF, 2, 6 (1962).

[8] Vaglio-Lauren, R., Ferri, A., Theoretical investigation of flow field about blunt-nosed bodies in supersonic flight. J. A. S., 25, 12 (1958).

[9] Belotserkovskiy, O. M., Calculation of flow about axisymmetric bodies with detached shock waves (Calculation formulas and flow field tables), VTs AN USSR, Moscow (1961).

[10] Godunov, S. K., Zabrodin, A. V., Prokopov, G. P., Differential diagram for two-dimensional non-stationary problems of gas dynamics and the calculation of flow with detached shock wave. Zh. VMMF, 1, 6 (1961).

[11] Babenko, K. I., Rusanov, V. V., Differential method for solving three-dimensional problems of gas dynamics. Transactions of the 2nd All-Union Conference of Theoretical and Applied Mechanics [Trudy II Vsesoyuz. S"ezda po Teoret. i Prikl. Mekhan. Moscow (1965).

[12] Chen, Bingmu, Approximate calculation of several kinds of thermodynamic functions of air under equilibrium conditions. Lixue [Mechanics], 3 (1977).

[13] Moretti, A., A fast, direct and accurate technique for blunt-body problems. General Applied Science Labs Inc., TR 583 (1966).

[14] Tinyakov, G. P., Investigation of three-dimensional supersonic flow about rotating ellipsoids. IAN USSR, Mekhanika, 6 (1965).

[15] Belotserkovskiy, O. M., Flow of supersonic stream of gas about blunt bodies (Theoretical and experimental research), VTs AN USSR, Moscow (1966).

[16] Telenin, G. F., Tinyakov, G. P., Method for calculating three-dimensional flow about axisymmetrical bodies with detached shock waves. VTs AN USSR, Moscow (1961).